ISSN 0016-7029, Geochemistry International, 2007, Vol. 45, No. 4, pp. 345–363. © Pleiades Publishing, Ltd., 2007.
Original Russian Text © A.I. Brusnitsyn, 2007, published in Geokhimiya, 2007, No. 4, pp. 390–410.

Associations of Mn-Bearing Minerals as Indicators of Oxygen Fugacity during the Metamorphism of Metalliferous Deposits

A. I. Brusnitsyn

Division of Geology, St. Petersburg State University, Universitetskaya nab. 7/9, St. Petersburg, 199034 Russia
e-mail: brusspb@yandex.ru

Received October 7, 2005

Abstract—The paper summarizes experimental and calculation data on the effect of oxygen fugacity on the origin of mineral assemblages in Mn-bearing rocks and demonstrates the possibility of application of these data to the reconstruction of conditions under which metalliferous deposits were metamorphosed. A new variant of the $T-\log f_{O_2}$ diagram is proposed for the Mn–Si–O system, which differs from previous ones by the location of the lines for the formation (decomposition) of braunite and tephroite. These two minerals are the most universal indicators of oxygen fugacity during the metamorphism of Mn-bearing deposits, because these minerals are widespread in nature and can be formed in diverse environments: braunite at high f_{O_2} values in the pore solution, and tephroite at low f_{O_2} values. The occurrence of Mn oxides and rhodonite (pyroxmangite) in a rock makes it possible to constrain the oxygen fugacity range. An original $T-\log f_{O_2}$ diagram is constructed for the Ca–Mn–Si–O system. As follows from this diagram, a Ca admixture expands the stability field of rhodonite toward higher oxygen fugacity values. Johannsenite can be formed in these rocks at even higher f_{O_2}. The stability of both minerals is constrained in the region of low f_{CO_2}. The paper reports data on the Fe–Si–O and Mn–Fe–Si–O systems and discusses the possibility of applying the results of experiments in the Mn–Al–Si–O system to the estimation of conditions under which andalusite, spessartine, and galaxite can be formed in Mn-bearing rocks. Data on the mineralogy of numerous Mn deposits metamorphosed under various *PTX* parameters indicate that the origin of Mn-bearing mineral assemblages depends not so much on the temperature and pressure as on the oxygen fugacity, which is, in turn, controlled primarily by the composition of the pristine sediments (the presence or absence of organic matter in them) and host rocks and depends on the permeability of the rocks to oxygen, the *P–T* conditions, and the duration of the metamorphic processes.

DOI: 10.1134/S0016702907040039

INTRODUCTION

Associations of minerals with Mn, an element of variable valence, are systematically employed to "measure" the oxygen fugacity during certain geological processes. These minerals are utilized particularly often to elucidate the conditions under which metalliferous deposits were metamorphosed [1–8 and others]. These estimates are underlain, first of all, by the results of the experimental study of the stability of Mn-bearing minerals and their assemblages at various *PTX* parameters and by analogous information provided by qualitative or quantitative thermodynamic calculations. Regretfully, the potentialities of this approach are still limited, mostly because of the scarcity of experimental studies on systems with Mn and the lack of reliable thermodynamic constants for most Mn-bearing minerals. Moreover, experimental and calculation studies deal mostly with pure phases, whereas most minerals have, conversely, variable compositions. Because of this, the conditions under which natural and synthetic compounds are formed can be notably different. However, in spite of these limitations, the bank of experimental data on Mn-bearing systems is gradually being appended, and, thus, more possibilities are being created for its application to the solution of petrological problems.

The aim of this publication was to systematize and generalize currently available experimental and calculation data on the influence of oxygen fugacity on the formation of Mn-bearing minerals, to assess various mineral assemblages as possible oxygen fugacity indicators, and to identify factors that control f_{O_2} during the metamorphism of metalliferous sediments.

ANALYSIS OF MINERAL ASSEMBLAGES

System Mn–Si–O

This relatively simple system makes it possible to simulate interactions between principal rock-forming minerals of Mn-bearing rocks (ores), and, hence, this system traditionally has attracted much attention [5, 9, 10, and others].

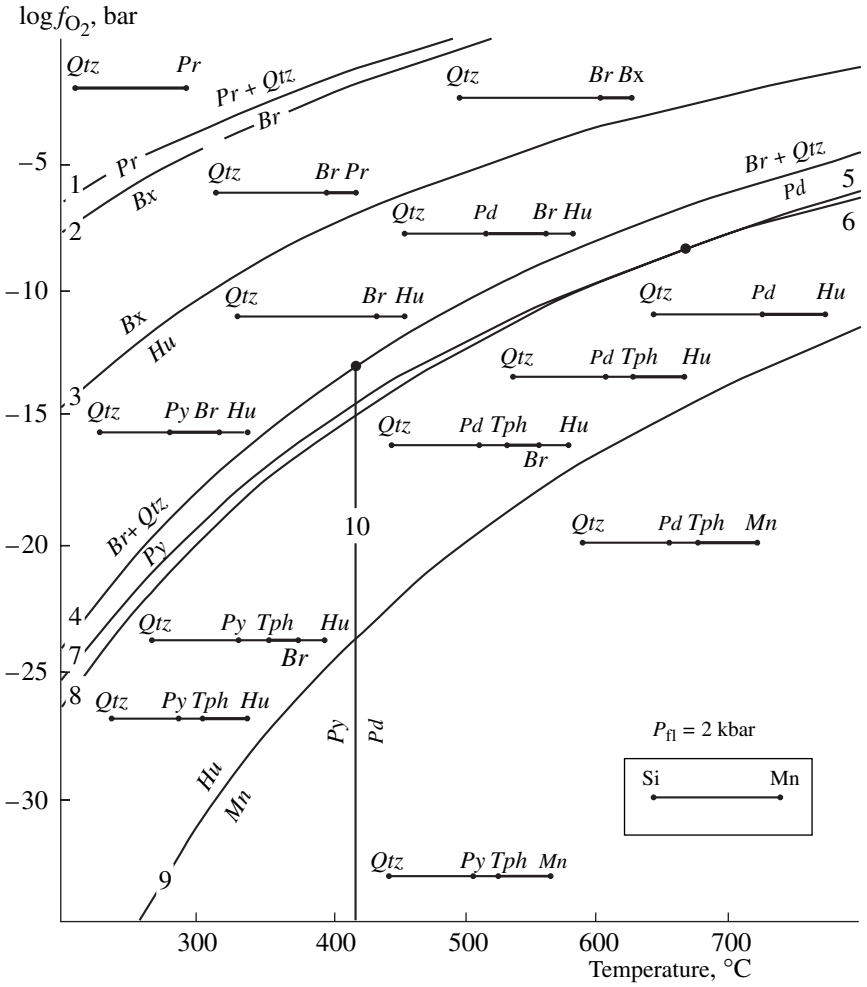

Fig. 1. $T-\log f_{O_2}$ diagram for the mineral assemblage in the Mn–Si–O system. Minerals: *Pr*—pyrolusite, *Bx*—bixbyite, *Hu*—hausmannite, *Mn*—manganosite, *Br*—braunite, *Rd*—rhodonite, *Py*—pyroxmangite, *Tph*—tephroite, *Qtz*—quartz. The heavy segments in the plots of mineral assemblages correspond to indicator associations (see text).

The model system comprises the following pure minerals: pyrolusite (*Pr*) MnO_2, bixbyite (*Bx*) Mn_2O_3, hausmannite (*Hu*) Mn_3O_4, manganosite (*Mn*) MnO, braunite (*Br*) Mn_7SiO_{12}, rhodonite (*Rd*) $Mn_5(Si_5O_{15})$, pyroxmangite (*Py*) $Mn_7(Si_7O_{21})$, tephroite (*Tph*) $Mn_2(SiO_4)$, and quartz (*Qtz*) SiO_2. The refined thermodynamic constants of these minerals are summarized in [10]. Using these data, we calculated the monovariant equilibria in the Mn–Si system and constructed a $\log f_{O_2}-T$ diagram at a constant pressure. The calculations were carried out in compliance with the conventional method [11–13], and the diagram is presented in Fig. 1.

The $T-\log f_{O_2}$ diagram was calculated for $P = 2$ kbar. At higher pressures, all the lines of monovariant equilibria shift toward lower oxygen fugacity values, but their shifts are very insignificant, 0.3 $\log f_{O_2}$ (bar) per 1 kbar of total pressure. As a rough approximation, the effect of pressure can be provisionally ignored.

This diagram displays two features that make it different from its earlier variants [4, 5, 8, 14, and others].

First, Fig. 1 shows two subparallel lines in the region of high oxygen fugacity corresponding to the reactions (1) 7 pyrolusite + quartz = braunite + 2 O_2 at the highest f_{O_2} and (2) 4 pyrolusite = 2 bixbyite + O_2 at lower f_{O_2}. In previous versions of this diagram, this succession of reactions was suggested only at $T-\log f_{O_2}$, with reaction (1) giving way to reaction (1a) 14 bixbyite + 4 quartz = 4 braunite + O_2 at higher temperatures. Correspondingly, the lines of all three reactions intersect at a point at 155°C (428 K) (Fig. 2). However, as was emphasized by the authors of the earlier variants of the diagram [5, 6], they used thermodynamic constants that needed to be refined, and the model constructed based on these constants is of a semiquantitative character. Calculations with the constants from [10] indicate that the lines of reactions (1) and (2)

can intersect at T = 100–800°C and P = 1–10000 bar only at $\log f_{O_2} \gg 0$ bar, i.e., at geologically implausible parameters.

Along with the results of calculations, the selection of a valid variant of a diagram should be warranted by its consistency with the results of mineralogical studies. In our situation, it is crucial to determine which of two mineral assemblages is stable: pyrolusite + braunite or bixbyite + quartz. If only the former assemblage is stable, the variant of the $T-\log f_{O_2}$ diagram shown in Fig. 1 is valid, and, if the later or both assemblages are stable, the earlier variant of the diagram displayed in Fig. 2 is correct.

The analysis of the factual material does not provide an unambiguous answer to this question: both assemblages were found in metamorphosed Mn-bearing sediments. The pyrolusite + braunite assemblage is widespread at the Shivariapur and some other ore deposits in western India [1, 5] and was reproduced experimentally at T = 600°C and P = 4 kbar [15]. At the same time, intergrowths of bixbyite and quartz are very rare, and these minerals are practically always separated by braunite or other phases. Moreover, according to Indian researchers [1], at least some braunite in these rocks crystallized before bixbyite. In other words, braunite is formed in these rocks not by reaction (1a) but by reaction (1).

With regard for the aforesaid, the variant of the $T-\log f_{O_2}$ diagram in Fig. 1 seems to be more plausible than the earlier variant, but the final choice requires further mineralogical and experimental research, which should take into account the actual chemical compositions of the minerals. In this context, it is interesting to recall the opinion of Robie et al. [10], who suggested that the stability of the associations in question depends on a possible Fe admixture in the system. Braunite is formed by the reaction of pyrolusite with quartz (reaction 1 in Fig. 1) at low Fe concentrations, and Fe-rich braunite can be produced by the reaction of Fe-rich bixbyite and quartz (reaction 1a in Fig. 2).

The other difference of the newly constructed $T-\log f_{O_2}$ diagram from its earlier versions is the position of the formation (or decomposition) reactions of tephroite.

It was previously thought that a decrease in the oxygen fugacity in the system results in the following succession of reactions: (5) 2 braunite = 2 rhodonite + 4 hausmannite + O_2 and (6) 6 rhodonite + 2 hausmannite = 6 tephroite + O_2, with the reaction lines remaining parallel throughout the whole temperature range. According to this model, the association of rhodonite and hausmannite is stable under broadly variable conditions and, hence, should be found at many deposits, whereas the assemblage of tephroite and braunite should not be found at all, which is, however, not the case.

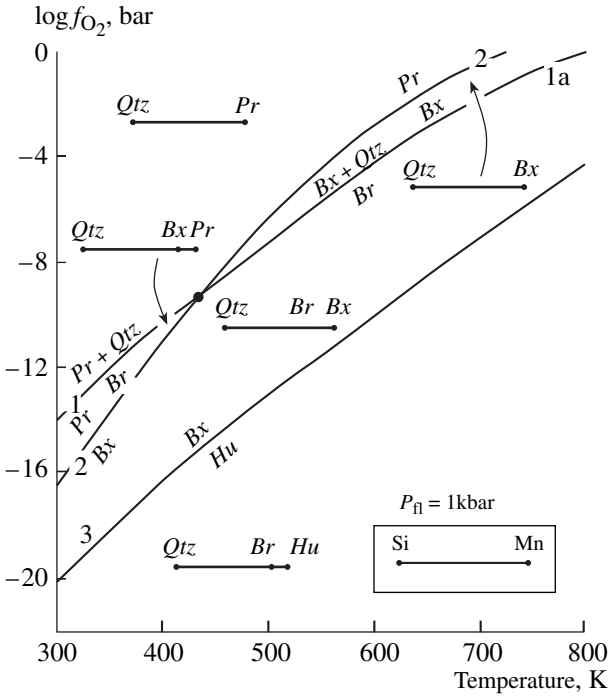

Fig. 2. $T-\log f_{O_2}$ diagram for a fragment of the Mn–Si–O system [5]. Minerals: *Py*—pyrolusite, *Bx*—bixbyite, *Hu*—hausmannite, *Br*—braunite, *Qtz*—quartz. Reaction numbers (1)–(3) correspond to those in Fig. 1.

Our calculations indicate (Fig. 1) that reactions (5) and (6) can take place only at high temperatures. At P = 2 kbar, the lines intersect at an invariant point at T = 670°C. Below this point, two other reactions occur: (7) 2 braunite + 10 rhodonite = 12 tephroite + 3 O_2 and (8) 3 braunite = 3 tephroite + 5 hausmannite + 2 O_2. Correspondingly, the assemblage of tephroite and braunite is stable at low temperatures and that of rhodonite and hausmannite is stable at high temperatures.

The results of our calculations are in good agreement with both experimental evidence and the results of mineralogical studies at several deposits. For example, Abs-Wurmbach and Peters [15] conducted a series of experiments and demonstrated that tephroite is formed by the reaction of braunite and rhodonite [reaction (7)] at $P > 1$ bar rather than via the interaction of rhodonite and hausmannite [reaction (6)]. This means that the assemblage stable at high pressures is that of tephroite + braunite but not rhodonite + hausmannite.

Both of these assemblages were found in nature, and both are rare. This is explained by the extreme narrowness of their stability fields (Fig. 1). The stability field of the tephroite and braunite assemblage is a narrow wedge. The wedge is bounded by reaction lines (7) and (8), and its width in terms of $\log f_{O_2}$ rapidly diminishes with increasing temperature. Even there, the tephroite + braunite pair can be formed only if the Mn/(Mn + Si) proportion in the rock is within the range of 0.67–0.88.

Otherwise, the stable associations are those of quartz + rhodonite (pyroxmangite), pyroxmangite + tephroite, and braunite + hausmannite. Nevertheless, syngenetic aggregates of tephroite and braunite were found in the rocks of at least two Mn deposits: the Noda-Tamagawa Mine in Japan [16] and on Paros Island in Greece [10]. The association of tephroite and hausmannite was thought to be formed by the decomposition of braunite on the strength of mineralogical evidence detected at the Semail Complex in Oman [17].

The association of rhodonite and hausmannite is also stable within a very narrow range of oxygen fugacity, in the field constrained by reaction lines (5) and (6) (Fig. 1). I am aware of a single find of this assemblage at the Sausar group of Mn deposits in India, whose rocks are metamorphosed to the amphibolite facies [1]. Moreover, hausmannite–rhodochrosite–rhodonite and hausmannite–rhodonite ores were described at two localities in the Russian Far East: in the Ir–Nimi interfluve area and on Bolshoi Shantar Island [18]. The authors characterize the relations of the hausmannite with rhodonite and rhodochrosite as reaction. Except these two examples, hausmannite has never been found in equilibrium assemblage with rhodonite, and they are always separated by tephroite, rhodochrosite, or other minerals [4, 15, 19, 20, and others].

Thus, the $T-\log f_{O_2}$ diagram in Fig. 1 is generally more consistent than the earlier variants with the naturally occurring mineral assemblages of the Mn–Si–O system.

The analysis of our variant of the diagram shows the following. Its whole $T-\log f_{O_2}$ space can be subdivided into two large sectors. The first of them is constrained by the lines of reactions (1), (8), and (5) and encompasses the region of $\log f_{O_2}$ values at which braunite is stable, one of the most widespread natural minerals of trivalent Mn. This sector corresponds to the stability of "oxidized" associations, which include, in addition to braunite, bixbyite, hausmannite, rhodonite (pyroxmangite), and quartz. This segment can be appended by the area above line 1, which includes no braunite but where the assemblage of pyrolusite + quartz is stable. The latter is, however, rare in metamorphic rocks and is more typical of hydrothermal, sedimentary, and supergene mineral deposits. The second sector is located in the lower part of the diagram, below the reaction lines 7 and 6. This region of relatively low $\log f_{O_2}$ values corresponds to the stability of tephroite and "reduced" associations and is dominated by minerals with bivalent Mn: tephroite, rhodonite (pyroxmangite), manganosite, hausmannite, and quartz. This sector also includes a wedge-shaped field between lines 5 and 6, which contains neither braunite nor tephroite. The sectors overlap within a very narrow field (between lines 7 and 8), which has a positive slope relative to the temperature axis: the higher the temperature, the wider the stability field of the "reduced" assemblages.

The sectors distinguished above provide rough characteristics of the conditions under which the two most widely spread types of metamorphosed Mn deposits are formed: (1) "oxide," whose principal minerals are braunite; oxides of tri- and, more rarely, tetravalent Mn; and quartz and (2) "silicate," which are devoid of braunite but contain widespread tephroite and other silicates of bivalent Mn; quartz; and, often, rhodochrosite. As follows from the diagram, hausmannite and rhodonite (pyroxmangite) can be contained in both rock types. Much of the rhodonite (pyroxmangite) stability field lies in the lower part of the $T-\log f_{O_2}$ diagram, which implies that pyroxenoids are still more typical of "reduced" associations of silicate rocks.

Both sectors comprise a number of segments separated by monovariant equilibrium lines. Each of the segments is characterized by its own set of mineral assemblages. Some of these assemblages are "endemic" (indicator) for certain segments and do not occur anywhere else in the diagram, while others are "telescoped" through broader ranges of parameters and can occur in more than one segment. For example, in the first (upper) sector, the braunite + bixbyite assemblage is stable exclusively within the field bounded by lines 2 and 3 and is the indicator assemblage of this segment. At the same time, the association of braunite ad quartz is stable over a broader field, which encompasses three segments of the diagram, from line 1 to line 4. Analogously, in the second (lower) sector of the diagram, the tephroite + hausmannite assemblage is the indicator assemblage for the segment between lines 8, 6, and 9. The telescoped tephroite + rhodonite (pyroxmangite) assemblage is, conversely, stable thought the whole lower sector. In Fig. 1, index mineral assemblages are indicated as heavy-line segments of the Mn–Si chemographic diagrams of mineral assemblages, and the telescoped assemblages are shown with thin lines.

As can be clearly seen in these diagrams, its subparallel segments have different widths. Moreover, the origin of mineral associations is controlled not only by temperature and oxygen fugacity but also by the Mn and Si proportions in the rocks. Because of this, the significance of various mineral assemblages as indicators of the $T-\log f_{O_2}$ parameters of geological processes is different. For instance, the find of the braunite and pyrolusite indicator assemblages in a metamorphic rock allows the researcher to fairly accurately constrain the oxygen fugacity in the environment (if the temperature and pressure were evaluated independently). In an analogous situation, the association of braunite and bixbyite constrains a much broader range of possible $\log f_{O_2}$ values. Even less information can be derived form the occurrence of the telescoped braunite and quartz assemblage. The rhodonite (pyroxmangite) + quartz assemblage marks only the upper $\log f_{O_2}$ limit of the metamorphic parameters. An analogous single constraint (but at lower oxygen fugacity) can be

deduced from the tephroite and rhodonite (pyroxmangite) assemblage or that of tephroite and manganosite.

In general, the comparison of mineral assemblages found in nature and those depicted in the $T-\log f_{O_2}$ diagram facilitates the evaluation of the f_{O_2} value during the metamorphism of Mn-bearing sediments (if the temperature and pressure are known). This approach is particularly efficient if the ore deposits have a broadly varying composition. Broad variations in the Mn/(Mn + Si) ratio of rocks are favorable for the origin of many mineral assemblages in them, and this enables the researcher to improve the accuracy of the constraints imposed on the oxygen fugacity. If the deposits are compositionally homogeneous in terms of Mn and Si concentrations, the potential of this approach is not as high. The more homogeneous the rock, the broader the $\log f_{O_2}$ range can be determined by its mineral associations. The uncertainty is particularly high if the rock contains relatively little Mn with Mn/(Mn + Si) > 0.5. The two assemblages stable at this proportion of Mn and Si are braunite + quartz and rhodonite (pyroxmangite) + quartz, which are stable practically throughout the whole diagram.

Other limitations in the application of the model diagram are related to the fact that it shows only the relations of pure minerals. The presence of isomorphic admixtures in the minerals can notably affect their phase relations. This problem can be partly solved by examining other, more complex systems.

System Ca–Mn–Si–O

The Mn–Si–O system considered above characterizes the most general phase relations in Mn-bearing rocks. The expansion of this system by the introduction of other components makes it possible to further specify and constrain the conditions under which some minerals and mineral assemblages are formed. In particular, the introduction of Ca makes it possible to refine the $T-\log f_{O_2}$ parameters of pyroxmangite and rhodonite stability.

In the system considered above, pyroxmangite and rhodonite were treated as polymorphic modifications of the Ca-free compound $Mn(SiO_3)$ that are stable at low and high temperatures, respectively. Although this assumption is often valid, both minerals at most deposits do contain Ca, with the Ca concentrations in pyroxmangite being commonly low: less than 5% of the sum of the cations. At the same time, the amount of Ca replacing bivalent Mn in rhodonite is most often much higher, up to 1 f.u. Hence, phase relations with rhodonite can be characterized more realistically in the system with three (Ca, Mn, and Si) but not two (Mn and Si) inert components. Furthermore, this triple system makes it possible to assay the conditions under which johannsenite, another widespread Mn silicate, is stable.

Inasmuch as no reliable thermodynamic constants are now available for calcic rhodonite and johannsenite, phase relations in the Ca–Mn–Si–O system can be now analyzed only qualitatively using the Schreinemakers–Korzhinskii approach [11, 21]. For simplicity, we constructed only the $T-\log f_{O_2}$ part of the diagram in which Mn-bearing pyroxenoids can be formed (or decomposed). In the previous diagram (Fig. 1), it corresponds to the region in the vicinity of reaction line 4. Because of this, the minerals included in the system are pyroxmangite (*Py*) $Mn_7(Si_7O_{21})$, rhodonite (*Rd*) $CaMn_4(Si_5O_{15})$, johannsenite (*Jh*) $CaMn(Si_2O_6)$, calcite (*Cc*) $CaCO_3$, braunite (*Br*) Mn_7SiO_{12}, hausmannite (*Hu*) Mn_3O_4, and quartz (*Qtz*) SiO_2.

The diagram (Fig. 3) represents many known natural associations of Mn minerals. It demonstrates that rhodonite is stable within a broad field, which is bounded by the lines of the decomposition reactions of this mineral into pyroxmangite, calcite, and quartz [reaction (4*a*)]; braunite, calcite, and quartz [reaction (4*b*)]; and johannsenite, braunite, and quartz [reaction (4*c*)]. Relative to the Ca-free pyroxenoid (pyroxmangite), the stability field of rhodonite is shifted toward higher temperature and oxygen fugacity. One of the most ubiquitous assemblage of Mn-bearing rocks is braunite + quartz + rhodonite (see triangular plots *1*, *2*, and *3*), which is stable above the monovariant equilibrium of braunite with quartz and pyroxmangite [reaction (4)], i.e., can be formed at somewhat higher $\log f_{O_2}$ values than those following from the $T-\log f_{O_2}$ diagram for the Mn–Si binary diagram (Fig. 1). In other words, the position of reaction line 4 corresponds to the minimum possible oxygen fugacity needed for rhodonite to appear in association with braunite and quartz.

The stability field of johannsenite occupies the right-hand part of the diagram and is constrained by the reaction lines of johannsenite decomposition into rhodonite, calcite, and quartz [reaction (4*d*)] and into braunite, calcite, and quartz [reaction (4*e*)]. According to the latter reaction, johannsenite can be produced at high temperatures and a higher oxygen concentration in the pore solution than that at which rhodonite and, particularly, pyroxmangite are formed. A temperature increase is associated with an increase in the f_{O_2} at which the pyroxene crystallizes. An association of johannsenite, braunite, and quartz stable under these conditions (triangular plot 4) was described, for example, at the Gambatesa and Molinello deposits in northern Italy [22]. The metamorphic parameters of these deposits were estimated at $T \approx 275$°C and $P \approx 2.5$ kbar. Hence, the minimum formation temperature of johannsenite determined by the line of reaction (4*e*) should be no lower than 275°C.

Since the model system includes carbonate (calcite), many of the phase equilibria are controlled not only by the temperature and oxygen fugacity but also by the CO_2 concentration in the solution (Fig. 4). Johannsenite

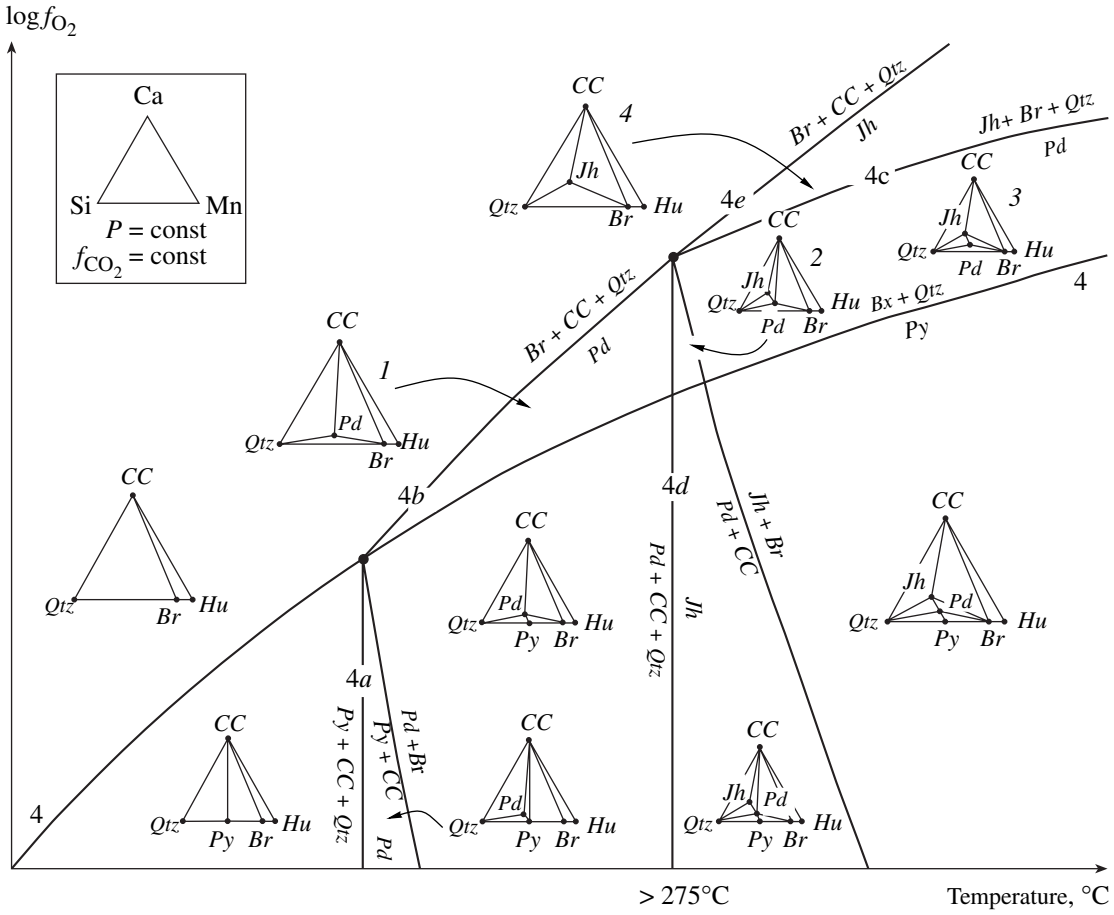

Fig. 3. Qualitative $T-\log f_{O_2}$ diagram for a fragment of the Ca–Mn–Si–O system. Minerals: *Hu*—hausmannite, *Br*—braunite, *Rd*—rhodonite, *Py*—pyroxmangite, *Jh*—johannsenite, *CC*—calcite.

and rhodonite can be stable at the lowest f_{CO_2} values in the rocks. An increase in the CO_2 fugacity results in the decomposition of, first, johannsenite [reactions (4*d*) and (4*e*)] and then rhodonite [reactions (4*a*) and (4*b*)]. The formation of pyroxmangite is independent of f_{CO_2} [reaction (*4*)].

The analysis of the $\log f_{O_2} - \log f_{CO_2}$ diagram (Fig. 4) clarifies why metamorphosed Mn rocks contain johannsenite much more rarely than rhodonite and pyroxmangite. The formation of the pyroxene requires, on the one hand, an elevated Ca concentration in the rock and, on the other, a low CO_2 concentration in the pore solution. However, Ca is usually introduced into the pristine rocks, together with CO_2, in the form of calcite. The CO_2 concentration in solution in equilibrium with these deposits is usually fairly high. Relatively high f_{CO_2} values are retained during metamorphism and preclude the formation of johannsenite. At the same time, the crystallization of rhodonite does not require either high Ca concentrations in the rock or too low CO_2 concentrations in the fluid, and these conditions are much more frequent.

As follows from the diagrams in Figs. 3 and 4, pyroxmangite, rhodonite, and johannsenite can coexist over a broad range of conditions. Metamorphosed Mn rocks only very rarely contain all three of them together, but the rhodonite + pyroxmangite or rhodonite + johannsenite pairs are spread quite widely.

Hence, the presence of Ca in Mn–Si deposits is favorable for the crystallization of rhodonite at an oxygen fugacity higher than in Ca-free rocks. Johannsenite can be formed in the same Ca–Mn–Si rocks at even higher f_{O_2} values. Moreover, the stability of both minerals (particularly, johannsenite) is limited by a low CO_2 concentration in the solution.

Fe–Si–O and Mn–Fe–Si–O Systems

Iron is a typical component of manganiferous deposits of sedimentary and hydrothermal–sedimentary genesis. Because of this, detailed diagrams of phase equilibria with the participation of Fe-bearing minerals can be successfully utilized to constrain the conditions under which Mn rocks were formed.

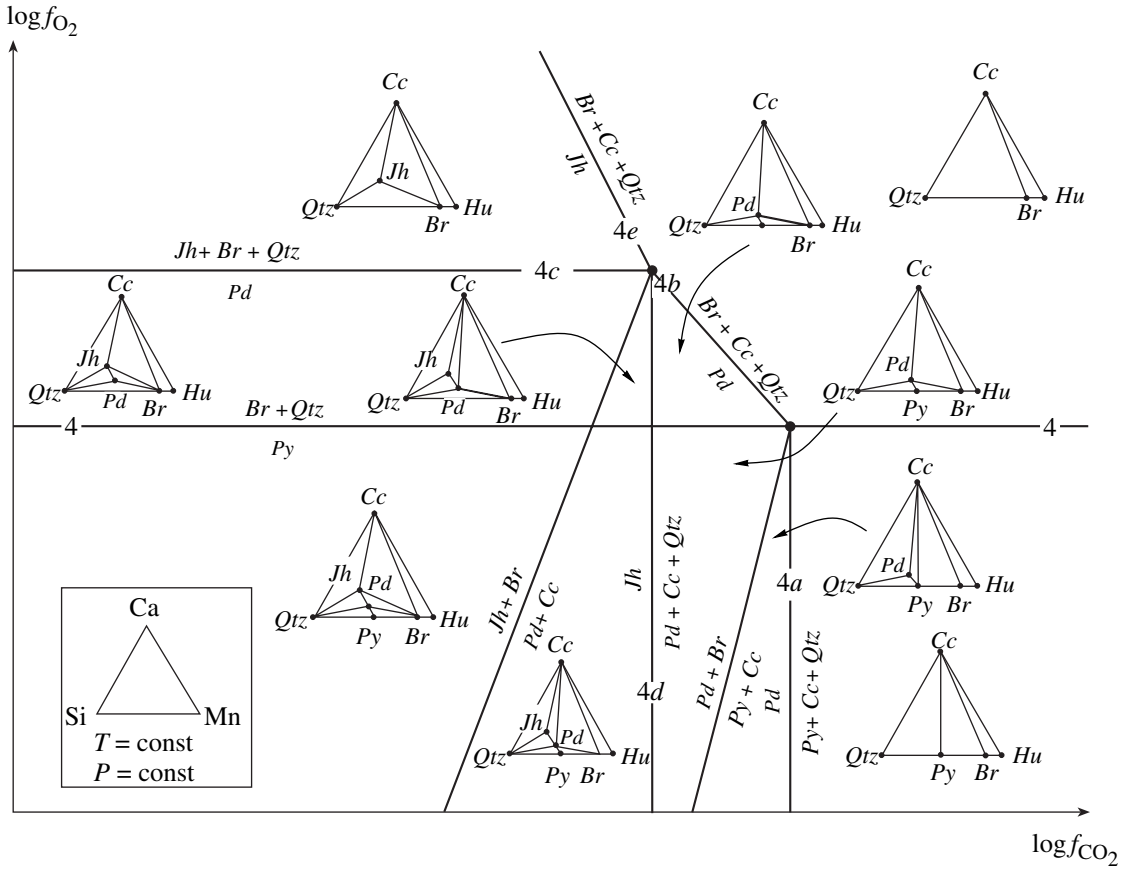

Fig. 4. Qualitative $\log f_{CO_2} - \log f_{O_2}$ diagram for a fragment of the Ca–Mn–Si–O system. Minerals: *Hu*—hausmannite, *Br*—braunite, *Rd*—rhodonite, *Py*—pyroxmangite, *Jh*—johannsenite, *Qtz*—quartz, *Cc*—calcite. The reaction numbers correspond to those in Fig. 3.

The location of the lines of key buffer reactions in the Fe–Si–O system is shown in the T–$\log f_{O_2}$ diagram in Fig. 5 (lines 11–16). Practically all of them pass below the equilibrium lines of Mn phases, and only the line of the magnetite/hematite buffer [reaction (11)] is situated above the reaction line 2 hausmannite = 6 manganosite + O_2 [reaction (9)]. Because of this, a typical Fe mineral in most Mn rocks is hematite. Magnetite appears in them much more rarely, and its occurrence testifies to reduced conditions. Magnetite commonly occurs in associations with rhodonite (pyroxmangite), tephroite, other silicates of Mn^{2+}, calcite, rhodochrosite, and hausmannite and/or manganosite. The coexistence of magnetite and hausmannite in rocks makes it possible to constrain the f_{O_2} values to a fairly narrow range.

In addition to the formation of individual phases, Fe is accommodated as an isomorphic admixture in Mn-bearing minerals. However, this component can be taken into account only qualitatively when the mineral equilibria are analyzed. It is thought that an admixture of Fe^{3+} shifts the bixbyite stability field toward higher f_{O_2}, and the shift for braunite is the opposite [1, 10]. The incorporation of significant Fe amounts into tephroite is possible only within a narrow range of conditions, within the stability field of fayalite $Fe_2(SiO_4)$. In the model diagram in Fig. 5, it corresponds to a region of very low f_{O_2} values between reaction lines 12 and 16. Above the magnetite + quartz/fayalite buffer [reaction (12)], the Fe concentration in tephroite should rapidly decrease. This explains why tephroite at the overwhelming majority of deposits bears extremely low Fe concentrations even at high concentrations of this element in the rocks. This mineral is formed at an oxygen fugacity above the stability level of the fayalite end member. Finds of Fe-rich tephroite (knebelite) point to very low f_{O_2} values under which these Mn rocks were formed.

A typical Fe mineral in Mn rocks is jacobsite (*Jc*) $MnFe_2O_4$. The conditions under which this mineral is stable were discussed by several researchers [1, 3, 5, and others]. However, practically all of these publications dealt only with some issues related to the genesis of certain associations. We attempted to partly bridge this gap and assay (at least qualitatively) the parameters at which many associations with jacobsite are stable. No quantitative calculations can still be conducted

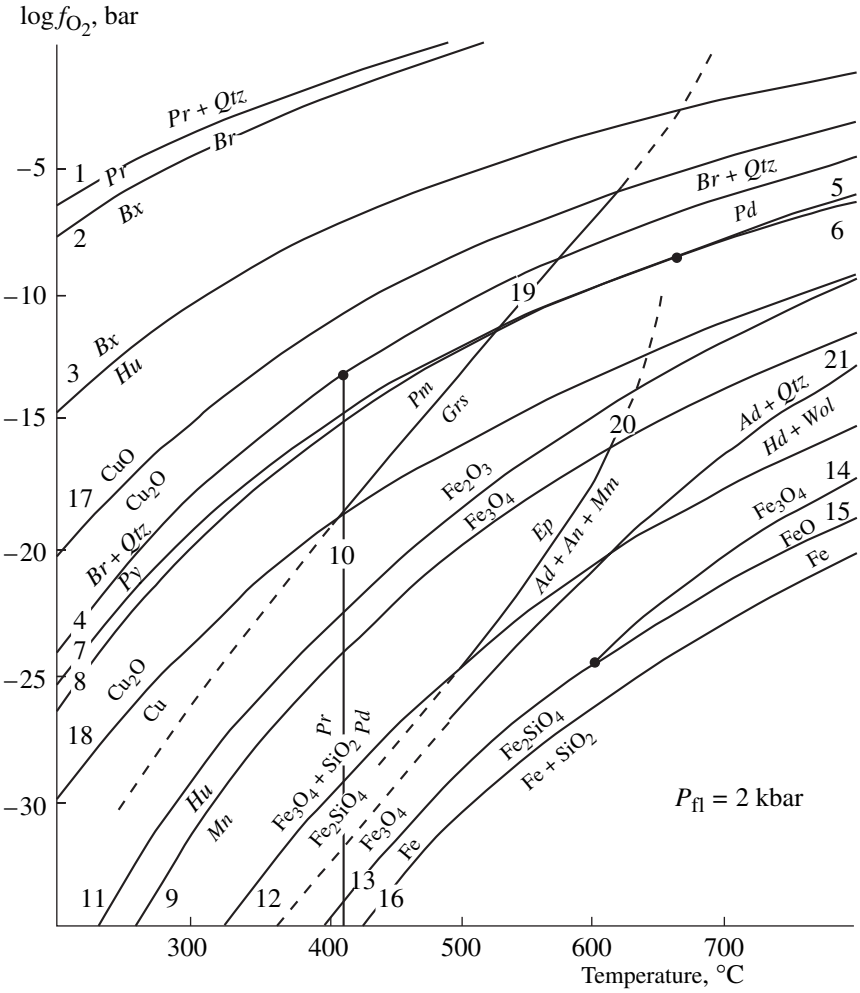

Fig. 5. $T-\log f_{O_2}$ diagram showing the stability of some Mn-, Fe-, and Cu-bearing minerals. Minerals: *Pr*—pyrolusite, *Bx*—bixbyite, *Hu*—hausmannite, *Mn*—manganosite, *Br*—braunite, *Rd*—rhodonite, *Py*—pyroxmangite, *Tph*—tephroite, *Qtz*—quartz, *Mt*—magnetite, *Pm*—piemontite, *Grs*—grossular, *Ep*—epidote, *Ad*—andradite, *An*—anorthite, *Wol*—wollastonite. Reaction numbers (1)–(10) correspond to those in Fig. 1.

because of the lack of reliable thermodynamic constants.

The diagram of phase equilibrium in the Mn–Fe–Si–O system (Fig. 6) is constructed for jacobsite and other phases having constant compositions. This diagram displays mineral assemblages above the magnetite/hematite buffer. These are, as was mentioned above, the most widely spread mineral assemblages of Mn-bearing rocks.

The line of the jacobsite-forming reactions [reactions (3*a*) and (3*b*)] have positive slopes relative to the temperature and oxygen fugacity axes. The higher the f_{O_2} value, the higher the crystallization temperature of this mineral. The stability field of jacobsite intersects the equilibrium lines of almost all Fe-free phases [reactions (3), (4), (7), and (8)] at acute angles, except the reaction lines with the participation of pyrolusite [reactions (1) and (2)]. Because of this, jacobsite can coexist with many leading Mn minerals but not with pyrolusite. This conclusion is in good agreement with the results of extensive mineralogical research. As can be seen in the $T-\log f_{O_2}$ diagram, compared to the associations of jacobsite with Mn silicates, the assemblage of jacobsite with quartz is formed at higher temperatures.

It is also interesting to mention the following noteworthy fact. Many jacobsite assemblages are stable at low temperatures and pressures, which correspond to low metamorphic grades or even premetamorphic grades of lithogenesis. For example, we found braunite-free rocks at the Kazagan-Tash deposit in the Southern Urals of Russia that simultaneously bear the jacobsite + tephroite and hematite + pyroxmangite assemblages (triangle plots *1* and *2*) and whose metamorphic conditions were assayed at $T \approx 250$°C and $P \approx 2.5$ kbar. The assemblages braunite + hausmannite + jacobsite (trian-

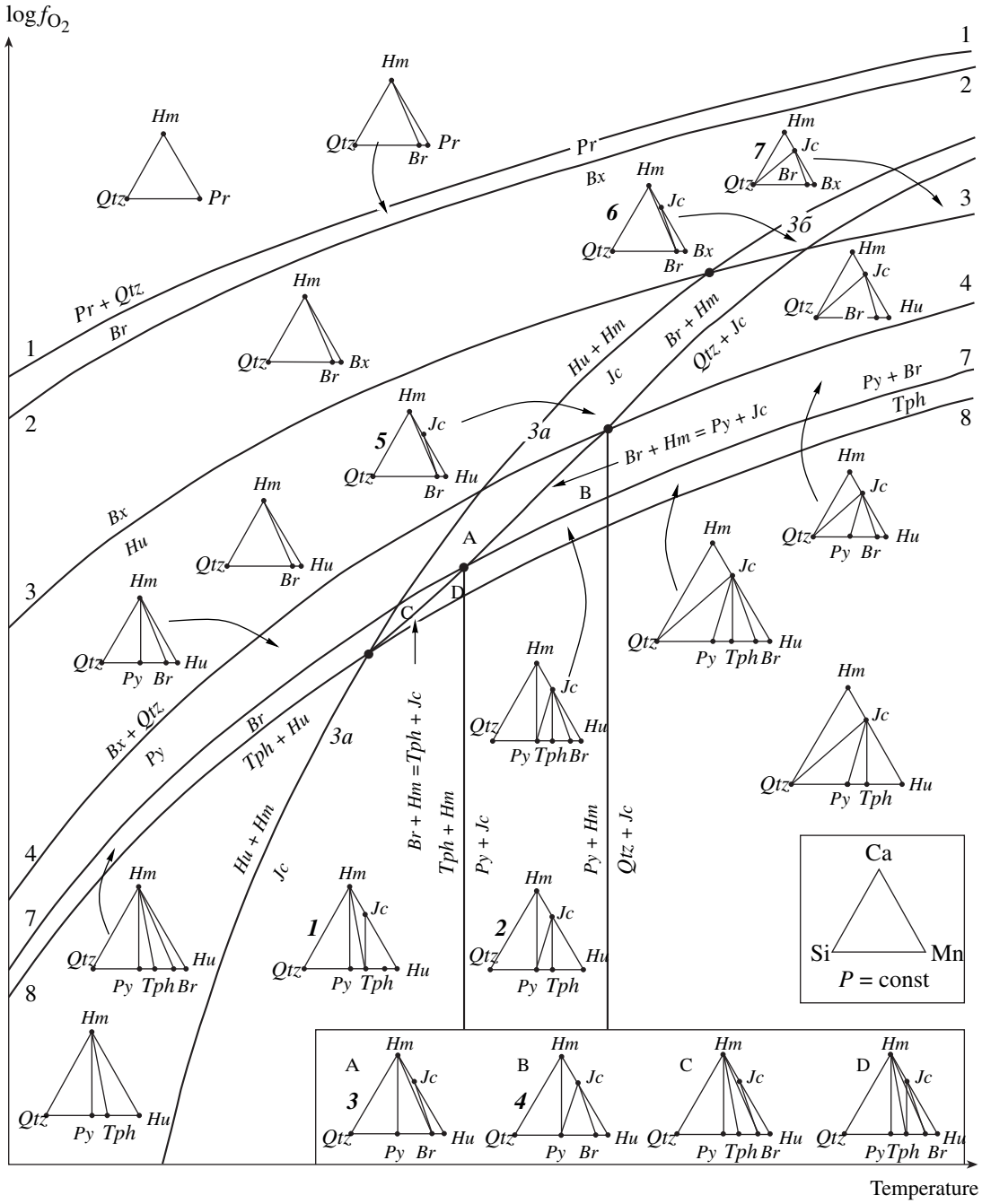

Fig. 6. Qualitative T– $\log f_{O_2}$ diagram for the Ca–Mn–Si–O system. Minerals: *Pr*—pyrolusite, *Bx*—bixbyite, *Hu*—hausmannite, *Br*—braunite, *Py*—pyroxmangite, *Tph*—tephroite, *Qtz*—quartz, *Hm*—hematite, *Jc*—jacobsite. Reaction numbers (1)–(4) and (7)–(8) correspond to those in Fig. 1.

gle plots *3*–*5*) and braunite + hematite + jacobsite (triangle plots *3* and *5*) are typical of tephroite-free Mn ores at deposits of the Mamatvan type in the Kalahari group in South Africa, which were metamorphosed at $T \approx 120$–200°C, $P \approx 1$ kbar [3]. This implies that the line of the reaction 2 hausmannite + 6 hematite = 6 jacobsite + O_2 [reaction (3a)] at f_{O_2} below that of the bixbyite/hausmannite buffer [reaction (3)] is located at temperatures lower than 200–250°C. Another indicator association, bixbyite + jacobsite (triangle plots *6* and *7*), is very rare and was reliably identified at the Otjosondu deposit in Namibia [23]. The metalliferous deposits are metamorphosed there to the amphibolite facies (T = 660–700°C, P = 5–6 kbar). Above the bixbyite/hausmannite buffer, jacobsite is likely stable at higher temperatures and pressures.

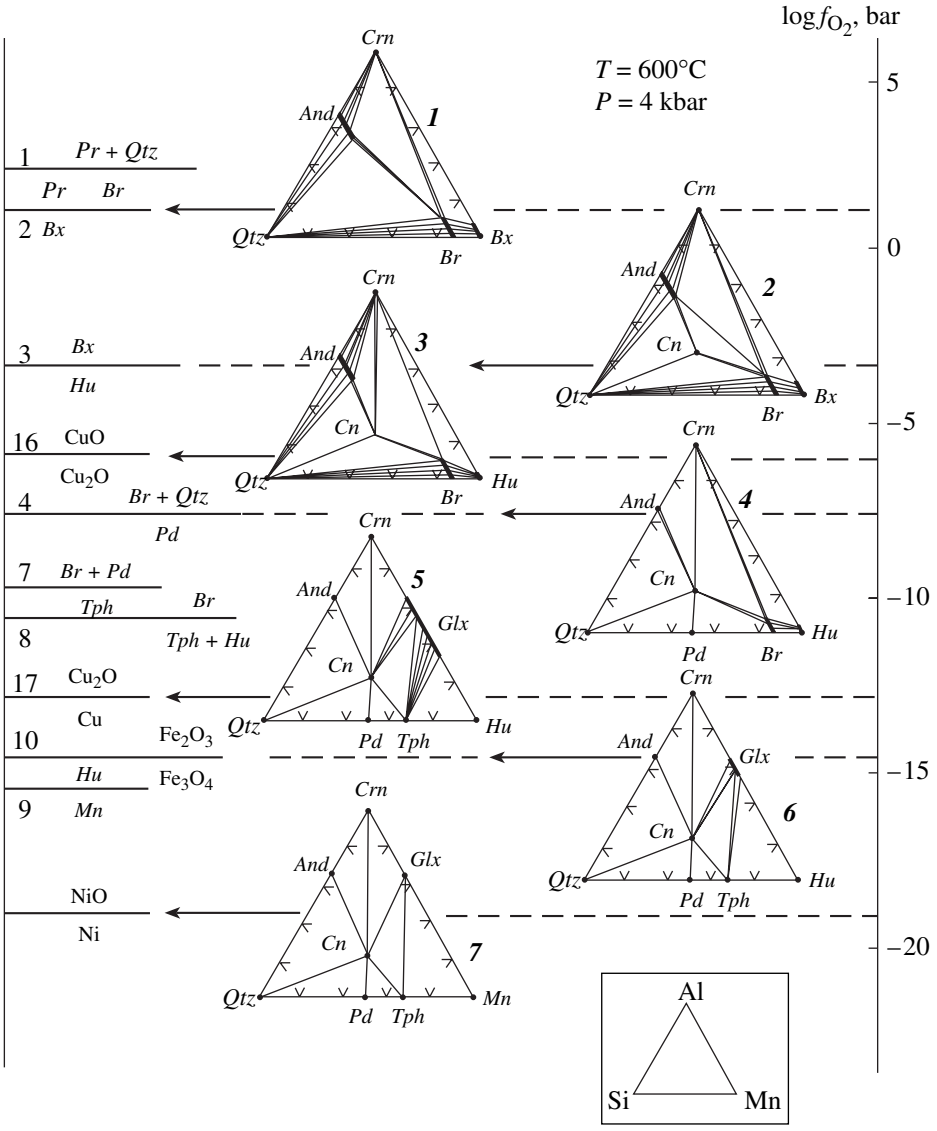

Fig. 7. Dependence of mineral assemblages in the Mn–Al–Si–O system on oxygen fugacity (based on the materials of [15]). Minerals: *Pr*—pyrolusite, *Bx*—bixbyite, *Hu*—hausmannite, *Mn*—manganosite, *Br*—braunite, *Rd*—rhodonite, *Tph*—tephroite, *Qtz*—quartz, *Crn*—corundum, *And*—andalusite, *Sps*—spessartine, *Glx*—galaxite. The reaction numbers correspond to those in Fig. 5.

Mn–Al–Si–O System

This system was studied experimentally by Abs-Wurmbach and Peters [15]. In an extensive series of experiments at a constant temperature (600°C) and pressure (4 kbar), they assayed the effect of oxygen fugacity on the formation of various associations of Mn minerals with corundum (*Crn*) Al_2O_3, andalusite (*And*) Al_2SiO_5, spessartine (*Sps*) $Mn_3Al_2(SiO_4)_3$, and galaxite (*Glx*) $MnAl_2O_4$. The principal results of this research are summarized in Fig. 7.

At f_{O_2} values corresponding to the bixbyite/pyrolusite buffer, the stable associations of the system are bixbyite + braunite + corundum, braunite + corundum + andalusite, and braunite + andalusite + quartz (triangle plot *1*). The latter assemblage was found in nature, for example, at the occurrences of Mn mineralization at the Venn Stavelot Massif in Belgium [24] and at Semail in Oman [17].

As f_{O_2} decreases to the bixbyite/hausmannite buffer, braunite, andalusite, and quartz start to react with one another and form spessartine, and the reaction 6 braunite + 36 andalusite = 14 spessartine + 22 corundum + 9 O_2 takes place near the Cu_2O/CuO buffer. As a result, braunite coexists in this f_{O_2} range with spessartine and quartz (triangular plots *2* and *3*). This association was found in metamorphosed Mn deposits on Andros Island in Greece [25], in the Iberian Belt in Spain [26], and in the Aldan Shield in Russia [27]. The Mn rocks of the Aldan Shield additionally contain aggregates of spessartine, quartz, and andalusite, along

with hausmannite and some other minerals. The associations of these rocks are represented by triangular diagram *3*.

Under conditions specified by the buffer reaction 2 braunite + 12 quartz = 14 rhodonite + 3 O_2 [reaction (4)], the system contains two other associations: braunite + spessartine + rhodonite and rhodonite + spessartine + quartz (triangular diagram *4*). Both of them (particularly the latter) are among the most widely spread assemblages of metamorphosed Mn-bearing rocks.

At f_{O_2} values between the Cu/Cu_2O and Ni/NiO buffers, braunite is unstable, and the associations with tephroite and galaxite are formed in place of this mineral (triangular plots *5*, *6*, and *7*). Aggregates of these minerals with each other and with sonolite, alleghanyite, hausmannite, spessartine, and some other phases were found at Mn deposits in California in the United States [19], in the Central Urals in Russia [28], in the Semail Massif in Oman [17], and elsewhere. As can be clearly seen in the diagram of Fig. 7, the composition of galaxite systematically evolves with decreasing oxygen fugacity: while this mineral contains up to 50 mol % of the hausmannite end member near the $MnMn_2O_4$ buffer, it becomes practically pure $MnAl_2O_3$ near the Ni/NiO buffer. Analogous systematic variations in the concentrations of minor elements were also determined for andalusite, braunite, and hausmannite, but these variations in galaxite are the most conspicuous.

Abs-Wurmbach and Peters emphasized that, although their experiments were carried out at high temperature and pressure, their results can be extrapolated to other *PT* parameters. Indeed, many of the associations reproduced in these experiments occur in nature in rocks of very diverse metamorphic grades, from prehnite–pumpellyite to blueschist and granulite facies.

The experiments confirmed the estimates of the conditions under which spessartine and galaxite are formed (these constraints were underlain only by mineralogical observations before these experiments). The former is stable over a very broad *PTX* field, and the latter crystallizes only at low f_{O_2}. Many of the associations represented in the model diagram of Fig. 7 were found in natural Mn rocks and can be used to assay the oxygen fugacity during the metamorphism of the corresponding metalliferous deposits.

The results of the experiments explain why spessartine most often coexists with rhodonite, tephroite, and quartz, and its association with braunite is relatively rare: Mn-bearing sediments usually contain only low Al concentrations, and their Al/(Al + Mn + Si) ratios usually do not exceed 0.1, with this value decreasing with increasing Mn concentration. During the metamorphism of these deposits at a high f_{O_2}, Al is preferably accommodated as an admixture in braunite, which can contain up to 15 mol % $MnAl_6SiO_{12}$ (see triangle diagram *3*). The crystallization of spessartine requires higher Al concentrations in the rock and/or lower Mn concentrations. Note that garnet occurs in them in varieties richer in quartz. At the same time, braunite is unstable at low f_{O_2}, and tephroite and rhodonite contain practically no Al. Because of this, if a rock contains even insignificant concentrations of this element, it forms an individual phase: spessartine (see triangular plots *5–7*). Moreover, low Al contents in Mn rocks predetermine the very rare occurrence of andalusite in them and the absence of corundum. At oxygen fugacity below the bixbyite/pyrolusite buffer, this element is practically completely incorporated into braunite and/or spessartine.

Other Systems

The metamorphism of Mn-bearing deposits with an admixture of terrigenous and volcanic material often produces piemontite (*Pm*) $Ca_2Mn^{3+}Al_2(Si_3O_{12})(OH)$ and/or epidote (*Ep*) $Ca_2Fe^{3+}Al_2(Si_3O_{12})(OH)$. The conditions under which these minerals are formed were experimentally studied by Keskinen and Liou [29]. They obtained equilibrium lines for piemontite with Mn-grossular (*Grs*) $(Ca_2Mn^{2+})Al_2(Si_3O_{12})$ [reaction (19)] and epidote with andradite (*Ad*) $Ca_3Fe_2^{2+}(Si_3O_{12})$, anorthite (*An*) $Ca(Al_2Si_2O_8)$, magnetite (*Mt*) $FeFe_2O_4$, and quartz [reaction (20)], which are shown in the $T-\log f_{O_2}$ diagram in Fig. 5. According to these data, piemontite is stable at high f_{O_2} and relatively low temperatures. Compared to it, the stability field of epidote is shifted toward lower f_{O_2} and higher temperatures. Correspondingly, minerals of intermediate composition should crystallize under conditions between the reaction lines of the decomposition of pure piemontite and epidote, i.e., the $Mn^{3+}_{VI} \leftrightarrow Fe^{3+}_{VI}$ substitution notably expands the stability field of piemontite.

The experimental data are in good agreement with mineralogical observations. It was noted that, at the same metamorphic *PT* parameters, piemontite with very low Fe concentrations can occur together with braunite, whereas Fe^{3+}-enriched piemontite is contained in braunite-free rocks, together with rhodonite, tephroite, andradite, Mg-pumpellyite, and other minerals. These relations are clearly pronounced, for example, at Mn deposits in the Southern Urals in Russia and the Iberian Belt in Spain [26]. Piemontite with the highest Mn^{3+} concentrations is a rare mineral, and Mn-bearing deposits commonly contain this mineral with comparable concentrations of Mn^{3+} and Fe^{3+} or even Mn-epidote, which contains notably more Fe^{3+} than Mn^{3+}. The stability field of this "standard epidote" covers practically the whole *PTX* range of low-grade metamorphism. Consequently, the occurrence of Mn-epidote suggests a relatively low metamorphic temperature but is poorly informative for constraining the oxygen fugacity.

Among the minerals of the garnet group, metamorphosed Mn-bearing rocks typically contain, along with spessartine, andradite, which crystallizes in rocks of various mineralogical composition throughout the practically whole *PT* range of metamorphic parameters. In the $T-\log f_{O_2}$ diagram of Fig. 5, andradite also occurs within a very broad stability field, whose lower boundary [reaction (21)] is located (according to the experimental data [30, 31]) near the magnetite–quartz/fayalite buffer. At lower f_{O_2} and/or higher temperatures, the association andradite + quartz is replaced by the association of hedenbergite (*Hd*) $CaFe^{2+}(Si_2O_6)$ with wollastonite (*Wol*) $Ca(SiO_3)$. By analogy with the minerals of the epidote group, it is reasonable to suggest that an admixture of Mn^{3+} in the silicates shifts the equilibrium line of this reaction toward higher f_{O_2} values.

Because andradite is stable within a very broad field of physicochemical parameters, it commonly cannot be used as an indicator of temperature, pressure, or oxygen fugacity of metamorphic processes. At the same time, the occurrence of andradite in rocks suggests a low f_{CO_2} in the mineral-forming solution. At a mole fraction of CO_2 higher than 0.1, the garnet decomposes into calcite, hematite, and quartz.

Another indicator of conditions under which Mn deposits are formed is native copper. This mineral was found in small amounts at many deposits and is typical mostly of Mn deposits of hydrothermal–sedimentary genesis localized in metamorphosed volcanic rocks. Examples of these deposits are the Bikkulovskoe deposit in the Southern Urals [32], Ir-Nimiiskoe and Shantarskoe deposits in Khabarovsk Krai in Russia [18], Otago in New Zealand [33], Gambatesa and Molinello in northern Italy [22], and others.

Native Cu is stable under relatively low oxygen fugacity (Fig. 5). The line of the Cu/Cu_2O buffer passes through the stability field of rhodonite (pyroxmangite) and tephroite above the line of the manganosite/hausmannite and magnetite/hematite buffers. Hence, the occurrence of native Cu poses the upper limit onto the f_{O_2} at which "reduced" associations of silicate Mn ores are formed. A still more informative association is that of native Cu with hematite and/or hausmannite, because these minerals can coexist only within a narrow range of conditions, and a temperature increase further diminishes this range. At the same time, Cu oxides (cuprite and tenorite) are stable at higher oxygen fugacity and are less informative genetically. Their occurrence in Mn deposits is related not so much to metamorphic processes as to the supergene replacement of metallic copper. If metamorphism proceeds at high f_{O_2}, Cu usually does not form individual phases but is accommodated as an isomorphic admixture in braunite, up to the formation of its cuprian analogue abswurmbachite $Cu^{2+}Mn^{3+}SiO_{12}$.

It is also pertinent to note that the occurrence of native copper in metamorphosed deposits points to a very low activity of sulfur in the pore solutions, because otherwise sulfides (first of all chalcopyrite) crystallize in place of native copper. The metalliferous sediments likely originally did not contain any sulfur compounds, and copper could accumulate in this sediment in the form of atacamite $Cu_2(OH)_3Cl$ and/or chrysocolla $Cu_4(Si_4O_{10})(OH)_4 \cdot nH_2O$. Both of these minerals are typical of hydrothermal Mn deposits in the modern ocean and decompose during metamorphism with the formation of native copper.

GENETIC INTERPRETATION OF THE RESULTS

The model diagrams presented in this paper make it possible to use the mineral assemblages of Mn rocks to constrain the physicochemical parameters under which these rocks were formed. For example, one can evaluate the oxygen fugacity during the metamorphism of metalliferous deposits. However, the following considerations should be taken into account when this information is used for petrological reconstructions.

The experiments and thermodynamic simulations were carried out for relatively simple systems and reproduced only some mineral assemblages of natural Mn-bearing rocks. The actual chemical composition of Mn-bearing deposits is much more complicated, and their mineralogy is much more diverse. Moreover, the addition of other components can notably modify the character of the mineral assemblages and the conditions under which they are formed. Because of this, experimental results don't always adequately characterize the conditions under which certain mineral deposits were produced. Experimental results can most often be interpreted qualitatively or semiquantitatively. Nevertheless, even this information is invaluable for genetic reconstructions.

With regard for these considerations, below we will analyze the regime of oxygen during the metamorphism of Mn-bearing deposits and try to identify factors that controlled it.

The typical mineral assemblages of Mn rocks generated under various *PTX* conditions are summarized in the table. For the sake of brevity, the table lists mainly deposits whose mineralogy was thoroughly examined in the past years and whose metamorphic parameters were evaluated by a number of independent techniques. The table reflects the mineralogy of main Mn orebodies but does not list the associations of younger veinlets (which are commonly relatively rare). The word *characteristic* is applied to mineral assemblages that provide quantitative information on the oxygen fugacity during their formation. The usage of this term in application to the Mn–Si–O system is wider than that of the term *indicator* (or *endemic*) association. *Other minerals* include all other phases found at the deposits, regardless of their abundances. The analysis of the data presented in the table leads to the following important conclusions.

Mineral composition of metamorphosed Mn-bearing rocks

no.	Deposit (country, region)	*PT* conditions	Characteristic mineral assemblage	Other minerals	Reference
			Premetamorphic facies of lithogenesis		
1	Bronkhorstfontein, Limpopo province, South Africa	$T < 200$°C	Braunite + quartz + hematite	Kaolinite, muscovite, chlorite	[34]
2	Mamatwan, Kalahary, South Africa	$T = 120$–210°C, $P \approx 1$ kbar	Hausmannite + braunite ± hematite ± jacobsite	Bementite, calcite, kutnahorite, and others	[3, 35]
			Facies of regional metamorphism A. Prehnite–pumpellyite facies		
3	Gambatesa and Molinello, Liguria, Italy	$T = 275 \pm 25$°C, $P = 2.5 \pm 0.5$ kbar	Braunite ± rhodonite + quartz ± hematite	Piemontite, parsettensite, rhodochrosite, and others	[22, 36–38]
			Braunite + rhodonite ± johannsenite + quartz	Manganaxinite, carpholite, caryopilite, parsettensite, calcite, rhodochrosite, and others	
			± Hausmannite + tephroite + rhodonite ± quartz ± hematite ± native Cu	Bementite, calcite, rhodochrosite, kutnahorite	
4	Smith Prospect and Manga–Chrome, California, United States	$T < 325$°C, $P < 2$ kbar	Hausmannite + tephroite + rhodonite + quartz + hematite ± jacobsite ± spessartine ± galaxite	Pyrophanite, sonolite, alleghanyite, caryopilite, clinochlore, pennantite, calcite, rhodochrosite, and others	[19]
5	Northern Fauzulinskoe, Southern Urals, Russia	$T \approx 250$°C, $P \approx 2.5$ kbar	Braunite ± rhodonite ± johannsenite + quartz ± hematite	Andradite, aegirine, aegirine-augite, winchite, magnesioriebeckite, parsettensite, albite, calcite, rhodochrosite, and others	Our data
6	Bikkulovskoe, Southern Urals, Russia	$T \approx 250$°C, $P \approx 2.5$ kbar	± Hausmannite ± tephroite, + rhodonite + johannsenite + quartz + hematite ± magnetite	Andradite, piemontite, epidote, pumpellyite, caryopilite, parsettensite, shirozulite, calcite, rhodochrosite, and others	[32]
7	Southern Fauzulinskoe, Southern Urals, Russia	$T \approx 250$°C, $P \approx 2.5$ kbar	Hausmannite + tephroite + rhodonite (+ pyroxmangite) + quartz ± hematite ± spessartine	Alleghanyite, ribbeite, caryopilite, pyrosmalite, talc, clinochlore, parsettensite, calcite, rhodochrosite, kutnahorite, and others	[20]
8	Kyzyl-Tash, Southern Urals, Russia	$T = 210$–280°C, $P \approx 2$ kbar	Huasmannite + tephroite + rhodonite + quartz + hematite ± magnetite	Andradite, epidote, manganaxinite, caryopilite, parsettensite, calcite, rhodochrosite, kutnahorite, and others	[39]

Table. (Contd.)

no.	Deposit (country, region)	*PT* conditions	Characteristic mineral assemblage	Other minerals	Reference
			B. Blueschist facies		
9	Buckey, California, United States	T = 150–200°C, P = 7–8 kbar	Hausmannite + braunite ± quartz	Gageite, taneyamalite, caryopilite, clinochlore, rhodochrosite	[19, 40]
10	Bonneval, France	T = 450–470°C, P = 6–8 kbar	Tephroite + rhodonite (pyroxmangite) + quartz, ± spessartine	Sonolite, alleghanyite, Na-amphibole, friedelite, rhodochrosite, kutnahorite, and others	[2]
11	Vitali, Andros Isl., Greece	T = 400–500°C, P = от 5–6 до >9 kbar	Braunite + quartz ± hematite ± spessartine	Hollandite, piemontite, titanite, cymrite, tremolite, muscovite, chlorite, albite, celsian, calcite, and others	[25]
			C. Greenschist		
12	Shivariapur, Kelkua-Rampura, Kailongy in Gujarat and other states of India	No data	Pyrolusite + braunite + quartz + hematite; Bixbyite + braunite + quartz + hematite ± spessartine	Hollandite	[1]
13	Santxan River, Taiwan	T= 475 ± 25°C, P = 3.5–4.5 kbar	Hausmannite + braunite + rhodonite + quartz ± spessartine	Mangancummingtonite, albite, celsian, rhodochrosite, kutnahorite	[41]
14	Deposits in the Iberian Peninsula, Spain	T = 450–500°C, P < 4 kbar	Braunite + quartz ± spessartine ± hematite	Epidote, piemontite, diopside, winchite, aegirine-augite, phlogopite, muscovite, albite, calcite	[14, 26]
			Hausmannite + tephroite + rhodonite + quartz ± spessartine	Actinolite, biotite, albite, calcite	
15	Cusma and Bistry Potok, Slovakia	$T \approx$ 400°C, $P \approx$ 3.5 kbar	Tephroite + rhodonite (+ pyroxmangite) + quartz ± spessartin	Actinolite, caryopilite, manganpyrosmalite, calcite, rhodochrosite, and others	[42]
16	Hoskins, Australia	T = 450–500°C, P < 4 kbar	Braunite + quartz	Aegirine, pectolite, kozulite, potassic feldspar, albite; calcite, and others	[4]
			Hausmannite + tephroite + rhodonite + quartz ± hematite ± magnetite	Andradite, hedenbergite, bustamite, caryopilite, pennantite, calcite, rhodochrosite, and others	
17	Malosedel'nikovskoe, Borodulinskoe, and other deposits in the Central Urals, Russia	T= 450–500°C, P = 2–3 kbar	Tephroite + rhodonite (+ pyroxmangite) + quartz + spessartine ± galaxite	Sonolite, alleghanyite, tremolite, mangancummingtonite, phlogopite, calcite, rhodochrosite, and others	[28, 43]
18	Deposits in the Venn Stavelot Massif, Belgium	T = 360–420°C, $P \approx$ 2 kbar	Braunite + quartz + andalusite; Quartz + spessartine + andalusite + hematite	Gahnite, ardennite, ottrelite, muscovite, and others	[15, 24]

Table. Contd.

no.	Deposit (country, region)	*PT* conditions	Characteristic mineral assemblage	Other minerals	Reference
			D. Amphibolite facies		
19	Otjosondu, Namibia	T = 660–700°C, P = 5–6 kbar	± Hausmannite + braunite ± rhodonite + quartz + hematite + jacobsite ± spessartine ± Bixbyite + braunite ± quartz +jacobsite	Hollandite, andradite, sillimanite, aegirine, aegirine-augite, magnesioriebeckite, winchite, kinoshitalite, muscovite, and others	[23]
20	Deposits of the Sausar group, Madhja Pradesh and Maharashta states, India	T = 650 ± 50°C, P = 6 kbar	Bixbyite + braunite + quartz + hematite ± spessartine ± jacobsite; Hausmannite + braunite ± rhodonite (± pyroxmangite) + quartz + hematite ± jacobsite ± spessartine Tephroite + pyroxmangite + quartz + jacobsite + spessartine	Hollandite, piemontite, aegirine-augite, winchite, magnesioriebeckite, tremolite, mangancummingtonite, kinoshitalite, albite, potassic feldspar, calcite, rhodochrosite, kutnahorite, and others Andradite, mangancummingtonite, rhodochrosite	[1, 5, 44–46, et al.]
21	Bald Knob, North Carolina, United States	T = 575 ± 40°C, P = 5 ± 1 kbar	Tephroite + rhodonite (± pyroxmangite) + quartz ± jacobsite ± spessartine ± galaxite	Pyrophanite, sonolite, manganhumite, magnancummingtonite, caryopilite, kellyite, calcite, rhodochrosite, and others	[47, 48]
22	Hutter Mine, Virginia, United States	T ≈ 575°C, P ≈ 4 kbar	Manganosite + hausmannite + tephroite + magnetite + jacobsite + galaxite	Manganhumite, kinoshitalite, kutnahorite, and others	[49]
23	Vittinki, Finland	T = 740 ± 30°C, P = 4–5 kbar	Tephroite + rhodonite (+ pyroxmangite) ± quartz ± magnetite ± spessartine	Manganocummingtonite, rhodochrosite	[7]
			E. Granulite facies		
24	Garbham and other localities, Andhra Pradesh, India	T = 850°C, P = 8.5 kbar	Hausmannite + braunite + quartz + jacobsite		[50]
25	Deposits in the Aldan Shield, Russia	No data	± Hausmannite ± braunite + quartz + hematite ± magnetite + spessartine	Cordierite, biotite, oligoclase, microcline, and others	[18, 27]
26	Deposits in the Semail Complex, Oman	T = 800–850°C, P = 6.5–9 kbar	Braunite + quartz ± hematite ± andalusite Pyroxmangite + quartz + spessartine; hausmannite + tephroite + galaxite	Pyrophanite, kanoite, donpeacorite Mn-amphibole	[17]
			Contact metamorphic facies cordierite – andalusite facies		
27	Noda-Tamagawa, Iwate, Japan	T≈ 750°C, P ≈ 3–4 kbar	Manganosite ± hausmannite + tephroite + rhodonite + quartz ± spessartine ± galaxite ± Hausmannite + braunite ± tephroite + rhodonite + + quartz	Pyrochlore, Mn-mica, rhodochrosite, alabandite, and others Na-pyroxenes, Na-amphiboles, and others	[16, 51]

Notes: Characteristic minerals are listed in order of their decreasing Mn concentrations; the "plus – minus" sign means that the mineral occurs sporadically and in relatively small amounts.

First of all, it can be seen that Mn rocks produced at the same temperatures and pressures can consist of different minerals. The rocks of all metamorphic facies include both "oxidized" associations, which are dominated by braunite, rhodonite, Mn oxides, and quartz, and "reduced" ones, which are made up mainly of tephroite, rhodonite, hausmannite, and quartz. Vice versa, identical or closely similar mineral associations could be generated under different *PT* parameters. For example, the assemblages braunite + hausmannite and braunite + quartz are known to occur already in relatively weakly metamorphosed sedimentary deposits and in rocks of all metamorphic facies, from the prehnite–pumpellyite to granulite. The association of tephroite with hausmannite; tephroite with rhodonite; and, particularly, rhodonite with quartz can be formed throughout the whole range of metamorphic *PT* parameters. The indicator assemblage braunite + rhodonite ± quartz is stable under conditions from the prehnite–pumpellyite through amphibolite facies, and the bixbyite + braunite association is stable at least within the greenschist and amphibolite facies. An analogous situation exists with the associations of spessartine, galaxite, piemontite, hematite, and many other minerals. For example, layers with braunite mineralization at the Northern Faizulinskoe deposit in the Southern Urals (table, no. 5) and at the Otjosondu deposit in Namibia (table, no. 19) are closely similar mineralogically, but the metamorphic parameters of these deposits were assayed at $T \approx 250$°C, $P \approx 2.5$ kbar and $T = 660$–700°C, $P = 5$–6 kbar, respectively. Analogous examples are also known for braunite-free rocks. For example, a practically identical mineral composition is typical of the Smith Prospect and Manga–Chrome deposits in California (table, no. 4) and the Bald Knob deposit in North Carolina (table, no. 21). However, the metamorphic grades of the former two is no higher than the prehnite–pumpellyite facies ($T < 325$ °C, $P < 2$ kbar), and that of the latter one corresponds to the amphibolite facies ($T = 575 \pm 40$ °C, $P = 5 \pm 1$ kbar).

All of these facts definitely indicate that the mineralogy of metamorphosed Mn deposits was largely controlled not by the temperature and pressure but the chemical composition of the rocks and the concentrations of components in the pore solutions. One of the crucial factors of the equilibria was definitely the oxygen fugacity, which predetermined the development of "oxidized" or "reduced" mineral assemblages.

Oxygen fugacity could, in turn, be controlled by several factors. As is well known, Mn is accumulated mostly in the form of oxides during sedimentation. These deposits contain much more oxygen than any of their host rocks. Because of this, the burial and metamorphism of these deposits could hardly be associated with the borrowing of oxygen from any external sources. Thus, the amount of oxygen could remain unchanged in a closed system, and this element could only be removed from an open system.

One of the principal factors that could control variations in the f_{O_2} was likely the occurrence of organic matter with hydrocarbons in the original metalliferous sediments. The decomposition of this matter was associated with oxygen consumption and the release of carbon dioxide. The efficiency of this process was controlled by the content of biogenic mater in the rocks. The higher the C_{org} concentration, the greater the oxygen amount required for its oxidation, and the more significant the f_{O_2} decrease in the system. The simultaneous increase in the CO_2 concentration in the solution facilitated the crystallization of rhodochrosite and other carbonates in the Mn-bearing deposits. Hence, the interrelated variations in the f_{O_2} and f_{CO_2} in the pore solution are clearly reflected in the mineral composition of the rocks. Indeed, "reduced" rocks that were produced at low f_{O_2} consist mostly of hausmannite, tephroite, rhodonite, garnets, and quartz and practically always contain rhodochrosite as a principal mineral. At the same time, "oxidized" braunite–rich rocks contain only very small amounts of rhodochrosite, which occur only locally.

Rhodochrosite was most probably formed already during the diagenesis of the metalliferous sediment. This follows from the fact that deposits with this mineral occur in sedimentary sequences and in rocks of all metamorphic grades, including the lowermost grades. Up to the parameters of the prehnite–pumpellyite facies inclusive, rhodochrosite aggregates retain their typically diagenetic textures (spherulitic, globular, colloform, etc.) and show obvious indications of the replacement of oxide minerals by this carbonate. Moreover, at least partial carbonatization could also take place later, during catagenesis, in response to the inflow of elision hydrocarbon fluids into the Mn-bearing deposits. This model was proposed for some deposits at the peripheries of oil and gas fields (for example, [52] and others). However, for most other deposits, particularly those spatially restricted to volcanic–sedimentary sequences, this model is either inapplicable at all or could hardly be plausible. In any event, the crystallization of rhodochrosite during the oxidation of biogenic matter and, correspondingly, a drastic decrease in f_{O_2} in the system occurred before the metamorphism of the deposits. The participation of organic hydrocarbons in the formation of the carbonate is also corroborated by the carbon isotopic composition of this mineral [53–55 and others].

During their further metamorphism, the reduced conditions generated during early lithogenetic stages were retained and facilitated the crystallization of tephroite, rhodonite, and many other silicates of Mn^{2+}. The development of various mineral assemblages was then controlled not so much by f_{O_2} as by the CO_2 concentration in the solution.

Manganiferous sediments often contain biogenic and chemogenic Ca carbonates. Their partial dissociation also provides CO_2, but this does not affect the O_2

concentration in the solution. Because of this, calcite can be contained in both types of Mn rocks: both "oxidized" and "reduced."

The metamorphism of Mn deposits devoid of organic matter is usually associated with the partial reduction of tetra- and trivalent Mn oxides at an unchanging generally high f_{O_2} level. The latter tends to decrease with increasing temperature and pressure. As can be seen from the table, pyrolusite is stable up to the *PT* conditions of the greenschist facies; bixbyite is stable at least within the amphibolite facies and, perhaps, at higher *PT* parameters; and braunite and its associations with andalusite are known to occur in metamorphic rocks of the granulite facies.

An insignificant decrease in the oxygen fugacity during the metamorphism of Mn deposits was often explained [1, 15, and others] by the fact that the system is not fully closed. The fluid coming from the host rocks variably dilutes the pore solutions of the Mn ores and thus decreases the oxygen fugacity. In this situation, the capacity of the oxygen buffers should have been eventually exhausted, and this led to the reduction of the phases. The decrease of the f_{O_2} also depended on the chemistry of the metalliferous sediments, their permeability to fluids, *PT* parameters, and the duration of the metamorphic processes.

It is also worth noting the following. Manganiferous sequences often contain associations stable at different values of oxygen fugacity (see table). For example, sequences of braunite-rich rocks often include lenses made up of tephroite, rhodonite, rhodochrosite, and other minerals. Sequences of Mn-bearing sediments can consist of rhythmically alternating braunite–bixbyite, braunite–hausmannite, and other varieties, and these mineral assemblages show no traces of reaction relations and look stable. These and other similar examples are quite numerous. Moreover, the orebodies (even the relatively thick ones) are usually not surrounded by halos of oxidized rocks. These facts obviously indicate that oxygen behaves as an inert component during the metamorphism of Mn-bearing rocks, and its concentration is controlled mostly by the composition of these rocks. Oxygen is not extensively exchanged between adjacent portions of the sequences, and its migration (if any) is possible only for small distances comparable with the thicknesses of individual layers and lenses. The inert behavior of oxygen during metamorphism was documented by many researchers and not only in Mn-bearing rocks [8, 15, 29, 56, and others]. The mineralogy of the latter just offers a good illustration of this obviously widespread phenomenon.

Hence, the generalization of extensive factual material indicates that oxygen fugacity during the metamorphism of Mn-bearing sequences was largely controlled by the original composition of the metalliferous sediments and other factors played a subordinate role. This offers the possibility to use mineralogical data to reconstruct the character of the metalliferous protolith and evaluate the conditions under which it was produced and modified.

CONCLUSIONS

1. The most universal mineral indicators of oxygen fugacity during metamorphism are braunite and tephroite, which are widespread but crystallize under different conditions: at high and low f_{O_2} in the pore solution for braunite and tephroite, respectively. These minerals rarely occur together. The presence of other minerals in a rock provides the possibility of further constraining the oxygen fugacity at which this rock was formed. In this context, the most informative assemblages are those of an Mn oxide + silicate: manganosite + tephroite, hausmannite + tephroite, hausmannite + braunite, bixbyite + braunite, and pyrolusite + braunite. These assemblages are, however, rare because they are formed in rocks with the highest Mn concentrations.

2. Hausmannite and rhodonite can coexist with both braunite and tephroite. The main part of the stability field of rhodonite (pyroxmangite) lies at low f_{O_2} values, and, thus, the association of pyroxenoids with tephroite and accompanying minerals is more characteristic. An increase in the Ca concentration in rhodonite expands its stability field toward higher f_{O_2} values. Johannsenite can be formed in the same rocks at still higher f_{O_2} values. The stability of rhodonite with johannsenite is limited by the region of low CO concentrations in the solution.

3. Except for the hausmannite/manganosite buffer, all the other phase transitions between Mn minerals occur at higher f_{O_2} than those of Fe minerals. The most ubiquitous Fe mineral is hematite. The coexistence of magnetite and hausmannite in rocks further constrains the f_{O_2} values to a narrow range.

4. The crystallization temperature of jacobsite in rocks produced at low f_{O_2} and containing tephroite is much lower than in rocks with high f_{O_2} and containing braunite and accompanying minerals.

5. Spessartine is stable within a broad field of *PTX* conditions, and galaxite crystallizes only at low f_{O_2}.

6. The occurrence of Mn-bearing epidote in a rock is indicative of a low metamorphic temperature but is pooly informative in terms of oxygen fugacity.

7. The presence of native copper in Mn-bearing rocks makes it possible to further constrain the f_{O_2} values at which the "reduced" mineral assemblages of tephroite, rhodonite, hausmannite, rhodochrosite, and other minerals were formed. An even more informative assemblage is that of native copper with hematite and/or hausmannite: these minerals can coexist only within a narrow range of conditions.

8. The mineralogy of Mn-bearing metamorphic rocks is more strongly controlled by the oxygen fugacity than by temperature and pressure. The oxygen fugacity during the metamorphism of Mn-bearing

rocks is, in turn, largely predetermined by the composition of the original metalliferous sediments. The occurrence of organic hydrocarbons in them significantly decreases the oxygen fugacity already during their dia- and catagenesis. At a further temperature and pressure increase, this facilitates the crystallization of tephroite, rhodonite, and other silicates of Mn^{2+}, as well as hausmannite and manganosite. When metamorphosed, manganiferous sediments devoid of organic matter give rise to rocks dominated by braunite, rhodonite, and Mn oxides. The data presented above indicate that mineralogical information can be used to identify the nature of the metalliferous protolith and to constrain the conditions under which the sediments were accumulated and transformed.

REFERENCES

1. H. S. Dasgupta and R. M. Manickavasagam, "Regional Metamorphism of Non-Calcareous Manganiferous Sediments from India and a Related Petrogenetic Grid for a Part of the System Mn–Fe–Si–O," J. Petrol. **22**, 363–396 (1981).
2. A. Mottana, "Blueschist-Facies Metamorphism of Manganiferous Cherts: A Review of the Alpine Occurrences," in *Blueschist and Eclogites*, Ed. by B. W. Evans and H. Brown, Geol. Soc. Am. Men. **164**, 267–299 (1986).
3. T. Miyano and N. J. Beukes, "Physicochemical Environments for the Formation of Quartz-Free Manganese Oxide Ores from the Early Proterozoic Hotazel Formation, Kalahari Manganese Field, South Africa," Econ. Geol. **82**, 706–718 (1987).
4. P. M. Ashley, "Geochemistry and Mineralogy of Tephroite-Bearing Rocks from the Hoskins Manganese Mine, New South Wales, Australia," Neues Jahrb. Mineral. Abh. **161**, 85–111 (1989).
5. S. Dasgupta, P. Sengupta, P. K. Bhattacharya, et al., "Mineral Reaction in Manganese Oxide Rock: *P–T–X* Phase Relations," Econ. Geol. **84**, 434–443 (1989).
6. S. Dasgupta, "*P–T–X* Relationships during Metamorphism of Manganese-Rich Sediments: Current Status and Future Studies," in *Manganese Mineralization: Geochemistry and Mineralogy of Terrestrial and Marine Deposits* Geol. Soc. Spec. Publ. **19**, 327–337 (1997).
7. F. Mancini, R. Alviola, B. Marshall, *et al.*, "The Manganese Silicate Rocks of the Early Proterozoic Vittinki Group, Southwestern Finland: Metamorphic Grade and Genetic Interpretations," Can. Mineral. **38**, 1103–1124 (2000).
8. V. T. Kazachenko and V. V. Kiselev, "Manganese Mineral Assemblages as Indicators of the Redox Conditions of Metamorphism of Metalliferous Deposits," Tikhookean. Geol. **23** (5), 81–100 (2004).
9. I. Abs-Wurmbach, Tj. Peters, K. Langer, and W. Schreyer, "Phase Relations in the System Mn–Si–O: An Experimental and Petrological Study," Neues Jahrb. Mineral. Abh. **146**, 258–279 (1983).
10. R. A. Robie, S. Huebner, and B. S. Hemingway, "Heat Capacities and Thermodynamic Properties of Braunite (Mn_7SiO_{12}) and Rhodonite ($MnSiO_7$)," Am. Mineral. **80**, 560–575 (1995).
11. V. A. Zharikov, *Principles of Physicochemical Petrology* (Mosk. Gos. Univ., Moscow, 1976) [in Russian].
12. A. G. Bulakh and V. G. Krivovichev, *Calculations of Mineral Equilibria* (Nedra, Leningrad, 1985) [in Russian].
13. R. G. Berman, "Thermobarometry Using Multiequilibrium Calculations: A New Technique with Petrological Application," Can. Mineral. **29**, 833–855 (1991).
14. J. Jimenez-Millan and N. Velilla, "Mineralogy and Geochemistry of Reduced Manganese Carbonate–Silicate Rocks from the Aracena Area (Iberian Massif, SW Spain)," Neues Jahrb. Mineral. Abh. **166**, 193–209 (1994).
15. I. Abs-Wurmbach and Tj. Peters, "The Mn–Al–Si–O System: An Experimental Study of Phase Relations Applied to Parageneses in Manganese-Rich Ores and Rocks," Eur. J. Mineral. **2**, 45–68 (1999).
16. T. Watanabe, S. Yui, and A. Kato, "Bedded Manganese Deposits in Japan, a Review," in *Volcanism and Ore Genesis*, Ed. by T. Tatsumi, (Univ. Tokyo, Tokyo,1970; Mir, Moscow, 1973), pp. 119-142.
17. E. Gnos and Tj. Peters, "Tephroite–Hausmannite–Galaxite from a Granulite-Facies Manganese Rock of United Arab Emirates," Contrib. Mineral. Petrol. **120**, 372–377 (1995).
18. L. I. Kulish and E. A. Kulish, *Metamorphic Manganese Complexes of the Russian Far East* (ITG DNTs RAN, Khabarovsk, 1974) [in Russian].
19. M. J. K. Flohr and J. S. Huebner, "Mineralogy and Geochemistry of Two Metamorphosed Sedimentary Manganese Deposits, Sierra-Nevada, California, USA," Lithos. **29**, 57–85 (1992).
20. A. I. Brusnitsyn and I. G. Zhukov, "The South Faizuly Manganese Deposit in the Southern Urals: Geology, Petrography, and Formation Conditions," Litol. Polezn. Iskop., No. 1, 35–55 (2005) [Lithol. Miner. Resour. **40**, 30–47 (2005)].
21. D. S. Korzhinskii, *Theoretical Principles of the Analysis of Mineral Assemblages* (Nauka, Moscow, 1973) [in Russian].
22. R. Cabella, L. Gaggera, and G. Lucchetti, "Isothermal–Isobaric Mineral Equilibria in Braunite-, Rhodonite-, Johannsenite-, Calcite-Bearing Assemblages from Northern Apennine Metacherts (Italy)," Lithos. **27**, 149–154 (1991).
23. B. Buhn, M. Okrusch, E. Woermann, *et al.*, "Metamorphic Evolution of Neoproterozoic Manganese Formation and Their Country Rocks at Otjosondu, Namibia," J. Petrol. **36** (2), 463–496 (1995).
24. T. Theye and A.-M. Fransolet, "Virtually Pure Ottrelite from Region of Ottre, Belgium," Eur. J. Mineral. **6**, 547–555 (1994).
25. T. Reinecke, "Crystal Chemistry and Reaction Relation of Piemontites and Thulites from Highly Oxidized Low Grade Metamorphic Rocks at Vitali, Andros Island, Greece," Contrib. Mineral. Petrol. **93**, 56–76 (1986).
26. J. Jimenez-Millan and N. Velilla, "Compositional Variation of Piemontites from Different Mn-Rich Rock-Types of the Iberian Massif (SW Spain)," Eur. J. Mineral. **5**, 961–970 (1993).

27. D. P. Serdyuchenko and N. K. Dmitrienko, "Manganese Axinite and Manganese Andalusite: Constitutional Features and Paragenetic Significance," in *Geology and Geochemistry of Manganese* (Nauka, Moscow, 1982), pp. 181–192 [in Russian].

28. A. I. Brusnitsyn, *Rhodonite Deposits of the Central Urals: Mineralogy and Genesis* (St. Petersb. Gos. Univ., St. Petersburg, 2000) [in Russian].

29. M. Keskinen and J. G. Liou, "Synthesis and Stability Relations of Mn–Al Piemontite, $Ca_2MnAl_2Si_3O_{12}(OH)$," Am. Mineral. **64**, 317–328 (1979).

30. W. I. Gustafson, "The Stability of Andradite, Hedenbergite and Related Minerals in the System Ca–Fe–Si–O–H," J. Petrol. **15**, 455–496 (1974).

31. J. S. Liou, "Stability Relations of the Andradite–Quartz in the System Ca–Fe–Si–O–H," Am. Mineral. **59**, 1016–1025 (1974).

32. A. I. Brusnitsyn, Yu. S. Balashova, O. V. Gavryutchenkova, et al., "Native Copper from Manganese Rocks of the Bikkulovskii Deposit in the Southern Urals," in *Proceedings of the 6th All-Russia Conference on Mineralogy of the Urals-2003, Miass, Russia, 2003* (Inst. Min. Ural. Nauch. Ts. RAN, Miass, 2003), Vol. 2, pp. 29–35 [in Russian].

33. Y. Kawachi, R. H. Grapre, D. S. Coombs, and M. Dowsf, "Mineralogy and Petrology of a Piemontite-Bearing Schist, Western Otago, New Zealand," J. Metamorph. Geol. **1**, 353–372 (1983).

34. J. Gutzmer, M. O. Schaefer, and N. J. Beukes, "Red Bed-Hosted Oncolitic Manganese Ore of the Paleoproterozoic Soutpansberg Group, Bronkhorstfontein, South Africa," Econ. Geol. **97**, 1151–1166 (2002).

35. J. Gutzmer and N. J. Beukes, "Mineral Paragenesis of the Kalahari Manganese Field, South Africa," Ore Geo. Rev. **11**, 405–428 (1996).

36. E. Bonatti, M. Zerbi, R. Kay, and H. Rydell, "Metalliferous Deposits from the Apennine Ophiolites: Mesozoic Equivalents of Modern Deposits from Oceanic Spreading Centers," Geol. Soc. Am. Bull. **87**, 83–94 (1976).

37. G. Lucchetti, "Tephroite from Val Graveglia Metacherts (Liguria, Italy): Mineral Data and Reaction for Mn-Silicates and Mn–Ca-Carbonates," Eur. J. Mineral. **3**, 63–68 (1991).

38. P. Marescotti and M. L. Frezzotti, "Alteration of Braunite Ores from Eastern Liguria (Italy) During Syntectonic Veining Processes: Mineralogy and Fluid Inclusions," Eur. J. Mineral. **12**, 341–356 (2000).

39. E. V. Starikova, A. I. Brusnitsyn, and I. G. Zhukov, *Paleohydrothermal Edifice of the Kyzyl Tash Manganese Deposit, Southern Urals: Structure, Composition, and Genesis* (Nauka, St. Petersburg, 2004) [in Russian].

40. J. S. Huebner, M. J. K. Flohr, and J. N. Grossman, "Chemical Fluxes and Origin of Manganese Carbonate–Oxide–Silicate Deposit in Bedded Chert," Chem. Geol. **100**, 93–118 (1992).

41. T. F. Yui, C. H. Lo, and C. W. Lee, "Mineralogy and Petrology of Metamorphosed Manganese-Rich Rocks in the Area of Santxan River, Eastern Taiwan," Neues Jahrb. Mineral. Abh. **3**, 249–268 (1989).

42. S. W. Faryad, "Mineralogy of the Mn-Rich Rocks from Greenschist Facies Sequences of the Gemericum, West Carpathians, Slovakia," Neues. Jahrb. Mineral. Mh. **10**, 464–480 (1994).

43. E. N. Perova, *Physicochemical Model of the Formation of the Metamorphosed Silicate Manganese Deposits* (St. Peterb. Gos. Univ., St. Petersburg, 2004) [in Russian].

44. S. Roy, S. Dasgupta, N. Majumdar, *et al.*, "Petrology of Manganese Silicate-Carbonate-Oxide Rock of Sausar Group, India," Neues Jahrb. Mineral. Abh. **12**, 561–568 (1986).

45. P. K. Bhattacharya, S. Dasgupta, G. Chattopadhyay, et al., "Petrology of Jacobsite Bearing Assemblages from Sausar Group, India," Neues Jahrb. Mineral. Abh. **159** (1), 101–111 (1988).

46. S. Dasgupta, S. Roy, and M. Fukuoka, "Depositional Model for Manganese Oxide and Carbonate Deposits of the Precambrian Sausar Group, India," Econ. Geol. **87**, 1412–1418 (1992).

47. G. A. Winter, E. J. Essene, and D. R. Peacor, "Carbonates and Pyroxenoids from Manganese Deposit near Bald Knob, North Carolina," Am. Mineral. **66**, 278–289 (1981).

48. M. J. K. Flohr, "Geochemistry and Origin of the Bald Knob Manganese Deposit, North Carolina," Econ. Geol. **87**, 2023–2040 (1992).

49. J. S. Beard and R. J. Tracy, "Spinel and Other Oxides in Mn-Rich Rock from the Hutter Mine, Pittsylvania County, Virginia, U.S.A.: Implications of Miscibility and Solvus Relations Among Jacobsite, Galaxite, and Magnetite," Am. Mineral. **87**, 690–698 (2002).

50. S. Dasgupta, Y. Hariya, and H. Miura, "Compositional Limits of Manganese Carbonates and Silicates in Granulite Facies Metamorphosed Deposits of Garbham, Eastern Ghats, India," Resour. Geol. Spec. Issue, No. 17, 43–49 (1993).

51. K.-I. Hayashi and M. El Rhazi, "Oxygen Isotope Study of Metamorphosed Manganese Deposits of the Nada-Tamagawa Mine, Northeast Japan," Econ. Geol. **98**, 181–189 (2003).

52. V. N. Kuleshov and Zh. V. Dombrovskaya, "Manganese Deposits of Georgia: Communication 2. Origin of the Manganese Ores, with the Chiatura and Kvirila Deposits as Examples," Litol. Polezn. Iskop., No. 4, 339–355 (1997) [Lithol. Miner. Resour. **32**, 295–309 (1997)].

53. J. R. Hein and R. A. Koski, "Bacterially Mediated Diagenetic Origin for Chert-Hosted Manganese Deposits in the Franciscan Complex, California Coast Ranges," Geology **15**, 722–726 (1987).

54. M. El Rhazi and K. Hayashi, "Origin and Formational Environment of Noda-Tamagawa Manganese Ore, Northeast Japan: Constraints from Isotopic Studies," Chem. Erde. **63**, 149–162 (2003).

55. V. N. Kuleshov and A. I. Brusnitsyn, "Isotopic Composition ($\delta^{13}C$, $\delta^{18}O$) and the Origin of Carbonates from Manganese Deposits of the Southern Urals," Litol. Polezn. Iskop., No. 4, 416–429 (2005) [Lithol. Miner. Resour. **40**, 364–375 (2005)].

56. *Metamorphic Facies*, Ed. by V. S. Sobolev (Nedra, Moscow, 1970) [in Russian].